Hybrid Au-SiO_2 Core-Satellite Colloids as Switchable SERS Tags

Denis Rodríguez-Fernández,[a] Judith Langer,[a] Malou Henriksen-Lacey[a] and Luis M. Liz-Marzán[a,b]*

[a]*Bionanoplasmonics Laboratory, CIC biomaGUNE, Paseo de Miramón 182, 20009 Donostia - San Sebastian, Spain;*
[b]*Ikerbasque, Basque Foundation for Science, 48013 Bilbao, Spain;*

KEYWORDS. Gold, self-assembly, multiplex, SERS, cells.

ABSTRACT: Au-silica self-assembled nanostructures are reported as multiplex surface enhanced Raman scattering (SERS) tags for bioimaging applications. These hybrid colloidal particles were obtained by hetero-assembly of Au-SiO_2 Janus particles with smaller Au spheres and two Raman active molecules that can be independently imaged by varying the wavelength of the excitation laser. The Janus structure of Au-SiO_2 not only directs the assembly but also provides physical separation of the Raman tags and colloidal stability thereby facilitating complete silica encapsulation. The bioimaging capabilities of this system are demonstrated through SERS mapping of individual cells.

INTRODUCTION

Raman spectroscopy is based on the inelastic scattering of monochromatic photons under excitation of characteristic vibrational modes of a molecule, polymer or material, offering the unambiguous determination of their chemical identity, geometrical structure or oxidation state. Raman scattering is an intrinsically weak process due to the low probability of scattering events, leading to very small cross sections ($\approx 10^{-30} m^2$). Notwithstanding, the local enhancement of the electromagnetic (EM) field close to plasmonic nanoparticles, when exposed to an external light source, can lead to the enhancement of Raman scattering cross sections by many orders of magnitude, which is known as surface enhanced Raman scattering (SERS).[1-5] When plasmonic nanoparticles are in close proximity, the enhancement of the EM field is even higher due to coupling of individual localized surface plasmon resonances (LSPRs), generating so called hot spots[6] and allowing even more sensitive detection, down to the single molecule detection limit.[7-15]

Analytical applications are often based on the detection of multiple SERS labels which can be distinguished by their individual spectral fingerprints. Common strategies aim at either the detection of molecules, parts of proteins or cells through direct scattering enhancement of the analyte or at an indirect detection of nanoparticle tags labeled with a Raman-active dye (also referred to as "color") acting as signal amplifier.[16-21] Dye-encoded SERS nanotags have also been proposed as a powerful tool for imaging cell cultures due to their high sensitivity even in complex media.[22-25] This application requires effective SERS nanotags with improved stability and no toxicity, e.g. by adequate coating of the tag. Natan and coworkers reported the fabrication and SERS performance of dye-labeled tags coated with a protective glass shell,[26] whereas Doering and Nie successfully synthesized silica coated dye-embedded nanoparticles.[27] The SERS brightness of the nanotags could be enhanced through labeling of the nanoparticle with resonant Raman reporter molecules.[28] Dual-wavelength surface enhanced resonance Raman scattering (SERRS) was applied to quantify five different DNA sequences with low detection limit using dye-labeled nanoparticles which were resonant for 514.5 or 632.8 nm excitation wavelengths.[29] Another strategy to increase the sensitivity of the nanotag comprises positioning the Raman label within a hot spot between two nanoparticles. Aggregation can be induced by the organic dye molecule itself forming multiparticle assemblies[30] or alternatively, by addition of salt to the labeled particles prior silica coating.[31] Controlled formation of nanoaggregates was also demonstrated using dithiols as linkers,[32-34] and cancer cells were recently imaged using silica-coated nanoparticle dimers labeled with 4-mercaptobenzoic acid (4-MBA).[35]

Special effort has been made to develop efficient SERS nanotags with non-invasive, in vivo multiplex imaging potential.[25, 36-39] Zavaleta et al. demonstrated the in vivo detection of 10 different separately injected nanotags and the distinction of 5 synchronously injected nanotags to a nude mouse.[37] Complex multi-color (=multi-functional) nanotags were recently designed for the combined application of analytical (imaging) methods where each color selectively acts as a label for a specific technique, e.g. fluorescence, SERS, photothermal imaging, MRI etc.[40-43] We propose here a synthetic procedure to prepare hybrid core-satellite colloidal particles comprising differently sized Au spheres in close contact. We loaded these particle clusters with two different dye molecules and then covered them with silica to fix and protect the nanostructures for use as nanoantennas in SERS imaging applications using living cells.

Although examples of similar structures can be found in the literature, such as dimers and trimers of ~100 nm Au particles,[44,45] or the more recently reported satellite particles prepared by a masking desilanization process,[46] our strategy exploits the Janus behavior of Au-SiO_2 particles to restrict the area where the assembly can be produced and therefore to achieve a better control over the final geometry.[47] This configuration additionally allows the controlled introduction of two different dyes at specific locations within the composite particles, 4-mercaptobenzoic acid (4-MBA) under the silica shell of the Janus particle and rhodamine B isothiocyanate (RhB) within the hot spots generated during

the assembly. Significant differences in the energy dependence of the molecular Raman scattering cross section permit the interference-free detection of the individual components by selecting the adequate excitation wavelength. As a result, both labels can be independently traced for SERS imaging purposes by simply varying the laser excitation color. We propose that our method is advantageous because it allows multiplex SERS imaging using a relatively simple colloid chemistry approach. The hybrid satellites described here serve as a proof of concept to demonstrate the capabilities of this type of assembled nanostructures and open the way to the development of new architectures with even higher complexity for future applications in sensing, diagnosis or drug delivery.

EXPERIMENTAL SECTION

Synthesis of the building blocks. Au nanospheres of 15 nm average diameter were prepared by means of Turkevich's method.[48] The as prepared particles were transferred into ethanol upon exchanging the capping agent to poly(vinylpyrrolidone) (PVP, M_w 10,000 g/mol). The particles were incubated for 24 h with the polymer (60 molecules/nm^2) at room temperature, then centrifuged at 6000 rpm and redispersed in ethanol adjusting the final [Au] to 0.42 mM.[49] The synthesis of Au-SiO_2 Janus nanoparticles was carried out as previously described.[50] First, 27 mL of Au@citrate spheres (40 nm av. diameter) were prepared, centrifuged at 2100g for 20 min, washed and dispersed in Milli-Q water (10 mL). The seeds ([Au] ~0.3 mM in the final mixture) were then added dropwise under vortex stirring to a mixture of 2-propanol (38 mL) and H_2O (12 mL), containing 4-MBA (400 µL, 5 mM in EtOH) and polyacrylic acid (PAA, 400 µL, M_w 250,000 g/mol, $6.45 \cdot 10^{-5}$ M in H_2O). After stirring for 30 min to induce self-assembly of the ligands over the surface, ammonium hydroxide (1.8 mL, pH ~ 11) was added under fast stirring, followed by dropwise addition of tetraethyl orthosilicate (TEOS, 12 mL, 8.96 mM in 2-propanol) and then stored for ~12h under slow stirring. The particles were then washed and transferred to ethanol as follows: 10 mL of the as synthesized particles were centrifuged at 2100g for 30 min. The supernatant was centrifuged again under the same conditions and precipitates were collected, washed with 5 mL of water and centrifuged at 1900g for 20 min. The supernatant was removed and the particles were added dropwise to 10 mL of absolute ethanol under sonication ([Au] = 0.247 mM).

Synthesis of the hybrid Au-SiO_2 Core-Satellites. The assembly experiments were carried out in quartz cells of 1 cm path length at room temperature. To 2.5 mL of absolute ethanol were added 32 µL of Rhodamine B isothiocyanate 10^{-5} M ($[RhB]_{Final}$ = $9.6 \cdot 10^{-8}$ M), 172 µL of Au_{15}@PVP (0.42 mM in Au, or $2.4 \cdot 10^{12}$ particles/mL) and 490 µL of Janus Au_{40}(PAA-MBA@SiO_2) (0.247 mM in Au, or $7.5 \cdot 10^{10}$ particles/mL). The amount of RhB was estimated to be 0.5 molecules/nm^2, taking into account the total available gold surface, considering half of the Janus particles and the Au_{15} spheres. After each addition the cell was shaken manually. The mixture was incubated for 2 h in the dark with no apparent aggregation, and then 140 µL of 1 mM HCl was added to initiate the assembly (pH changes from ~8.5 to 5) (NOTE: the amount of HCl may vary when using different stock solutions of Au_{40}(PAA-MBA@SiO_2) Janus particles due to slight differences during the washing steps and subsequent transfer to ethanol). After several minutes while monitoring the spectral evolution in the visible, the process was detained by adding 90 µL of ammonia. The solution was then transferred to a glass vial and 800 µL of Milli Q water and 133 µL of TEOS (0.15 M in EtOH) were added while magnetically stirring the mixture. After 30 s the solution was stirred slowly for 2 h to complete the encapsulation. The assembled structures were washed 4 times with 1 mL of EtOH to remove silica nuclei, recovering them by centrifugation at 2100g for 30 min, and finally were dispersed in 1 mL of EtOH, storing them in the dark to minimize dye photobleaching.

All reactants were purchased from Sigma-Aldrich otherwise indicated.

Cell culture. J774 macrophages were purchased from ATCC (LGC Standards, Barcelona) and were cultured in DMEM media supplemented with 5% fetal bovine serum (FBS) and 1 % penicillin-streptomycicn (PS). Cells were maintained in humidified atmosphere at 37 ºC, 5% CO_2 and passaged using pipetting. All reagents were purchased from Invitrogen.

SERS of particles in cells. Cells were detached from growth flasks, counted and plated in a specially made cell slide comprising a normal microscopy glass slide or Suprasil Quartz glass to which a micro-chamber made of PDMS was glued. The surface area of each microchamber was approximately 0.5 cm^2, to which 8000 cells were added in a volume of 200 µL. Once attached, (no functionalization of the glass was needed), medium was replaced with PBS (10 mM, pH 7.4) and the sample was ready for viewing background levels. For SERS imaging of particles within cells, culture medium was removed and 15-30 µL of particles, suspended in PBS, was added to the well and left for 1 h at 37 °C. After 1 h the samples were washed using PBS and SERS maps were recorded. For experiments in which SERS signal measurements at 785 nm were involved, a special Suprasil Quartz glass was used (thereby minimizing background fluorescence).

Raman/SERS spectroscopy. Raman/SERS spectra and corresponding maps were recorded using a Renishaw InVia confocal Raman spectrometer coupled to a Leica DM-LM microscope and equipped with three different excitation lasers with wavelengths of 532 nm, 633 nm and 785 nm as well as two CCD cameras as detectors. SERS spectra of the Janus particles with and without satellites were recorded within 1 mm quartz UV cells using 1800 (532 and 633 nm) or 1200 lines/mm (785 nm) gratings and a long-distance 50x objective with a numerical aperture (NA) of 0.45. The integration time was set to 10s. The laser powers measured at the focus distance through the objective were 1.1 mW for 532 nm, 6.0 mW for 633 nm and 11.0 mW for 785 nm. The spectra (except at 532 nm) were background corrected and an off-set was applied for better clarity. SERS spectra of encoded Janus particles in J774 macrophage cells were collected with a 40x immersion objective (NA=0.85), in combination with a 600 lines/mm grating by measuring with an integration time of 0.5 s over the selected x-, y-range at each point of the grid (spacing of $\Delta x = \Delta y = 2$ µm) using a motorized microscope stage. For these measurements, laser powers of 2.0 mW (532 nm), 0.5 mW (633 nm) and 16.1 mW (785 nm) were applied. Two-dimensional SERS maps were created by plotting the baseline corrected intensity of characteristic vibrations at

each point as a function of grid position. The normalized SERS intensities were displayed on a rainbow-colored code from black (low intensity, I= 0-5) through violet (I = 5-15), blue (I = 15-30), lila-white (I = 30-40), green (I = 40-60), yellow (I = 60-65), orange (I = 65-70) and red (I > 70).

Instrumentation. Visible-NIR spectra were measured from 1 cm path length quartz cuvettes in an Agilent 8453 spectrophotometer. Transmission electron microscopy (TEM) analysis was performed with a JEOL JEM 1400F transmission electron microscope operating at an acceleration voltage of 120 kV.

RESULTS AND DISCUSSION

Scheme 1 summarizes the synthetic procedure used for the production of Au-SiO_2 hybrid satellites. Au spheres with an average diameter of 15 nm (Au_{15}), uniformly covered with poly(vinylpyrrolidone) (Mw = 10 kg/mol, PVP), and Au-SiO_2 Janus particles comprising a 40 nm Au core and a silica semishell, both dispersed in ethanol, were employed as building blocks (see Experimental Section for synthetic details). The Janus nanoparticles were prepared following a previously reported procedure, using both 4-mercaptobenzoic acid (4-MBA) and polyacrylic acid (PAA) as ligands, to grow a silica semishell over the 4-MBA covered part of the Au surface (Figure 2A).[50, 51] Both types of particles were first incubated with Rhodamine B isothiocyanate (RhB, $9.6 \cdot 10^{-8}$ M) in ethanol. This Raman reporter was selected because it features a high Raman cross section, as well as an isothiocyanate group that facilitates adsorption to gold particles, even when covered by a polymer shell, and high stability in both acidic and basic media within the pH range between 5 and 11. We thus expect that RhB adsorbs on both the small Au_{15} spheres and the exposed Au surface of the Janus particles (1 molecule per 2 nm^2 of total Au surface available).[52]

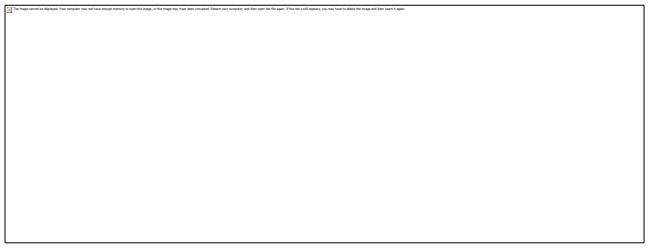

Scheme 1. Rhodamine B isothiocyanate (RhB) is incubated with Au_{15}@PVP spheres and Janus Au_{40}(PAA-MBA@SiO_2) particles. Self-assembly occurs when the pH is set to 5 and can be detained by increasing solution pH. A silica shell is finally grown to stabilize the hybrid nanostructures.

Therefore, two Raman active species are incorporated within the final nanostructures: RhB in the hot spots generated at the gaps between assembled Au particles, and 4-MBA at the Au-silica interface of the Janus nanoparticles. Importantly, addition of the dye did not trigger aggregation of the particles, as indicated by UV-vis spectroscopy (Figure 1). Aggregation did not occur because of the basic pH of the mixture (pH~8.5), at which PAA is deprotonated, thereby providing electrostatic stability. However when the pH was decreased to 5 via addition of 1 mM HCl_{aq}, aggregation started through van der Waals forces and electrostatic attraction between PVP and PAA due to the protonation of PAA (pKa ~ 4.8).[53] The assembly is indicated by redshift and broadening of the plasmon band, due to plasmon coupling (see Figure 1).[46, 54] Although a sufficient amount of Au_{15} spheres were added to cover ~80% of the available Au surface at the Janus particles, the assembly process was stopped after 5 minutes (by adding ammonia, increasing the pH of the mixture to ~11) to avoid the formation of bigger clusters comprising three or more Janus particles. It is interesting to note that no clusters comprising Au_{15}@PVP only were observed in TEM images, but instead they are always found to adsorb on Janus particles, either forming hybrid satellites or acting as bridges to produce dimers or bigger clusters. The low particle concentration in the TEM image in Figure 2B is due to the process used to avoid excessive particle aggregation during drying on the carbon-coated grid. As the assembly is a fast and dynamic process, five drops (8.5µL each) were casted on the grid, which was placed over paper. The paper support absorbed the excess of solution thereby providing more separated particles as well as a more realistic idea of what was present in solution.

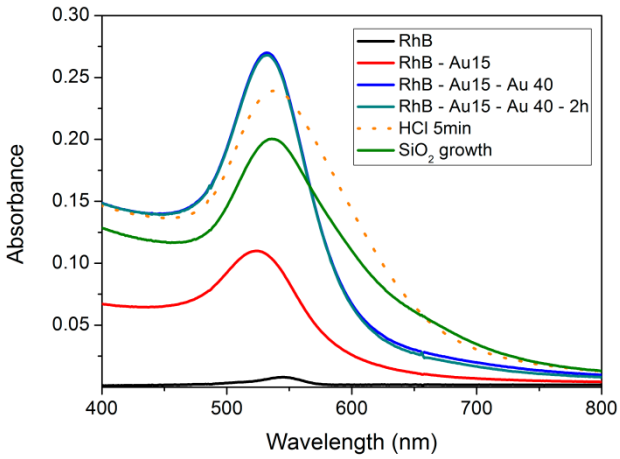

Figure 1. Spectral evolution during assembly and silica encapsulation.

Since the assembled nanoparticles are dispersed at high pH, silica shells can be grown using the well-known Stöber method,[55] so as to fix and protect the obtained structures (Figure 2C,D). Growing the silica shell immediately after completing the assembly helps preventing the dissolution of the silica semishell from the Janus nanoparticles. The final outer shell is stable in ethanol for extended periods of time and at least for one month in water, with no apparent dissolution as seen by TEM. Figure 2C,D shows representative TEM images of the final hybrid satellites after washing to remove excess organic molecules. Various types of particles can be clearly seen, including satellites made of one Janus particle and a few small spheres, dimers comprising two Janus particles linked by small Au_{15} spheres and some silica nucleation. The latter and the non-assembled Au_{15} spheres can be easily removed by 4-fold centrifugation and washing with ethanol. Analysis of ~500 particles revealed that ca. 49% hybrid satellites comprise one Au_{40} core with at least one Au_{15} particle, whereas 23% are Au_{40} dimers, 24% non-assembled Au_{40} particles, and some 4% are larger clusters, all of them covered with silica. This variation in the nanoarchitecture of the particles may lead to some differences in the plasmonic response and enhancing efficiency but is of little relevance to imaging as shown below.

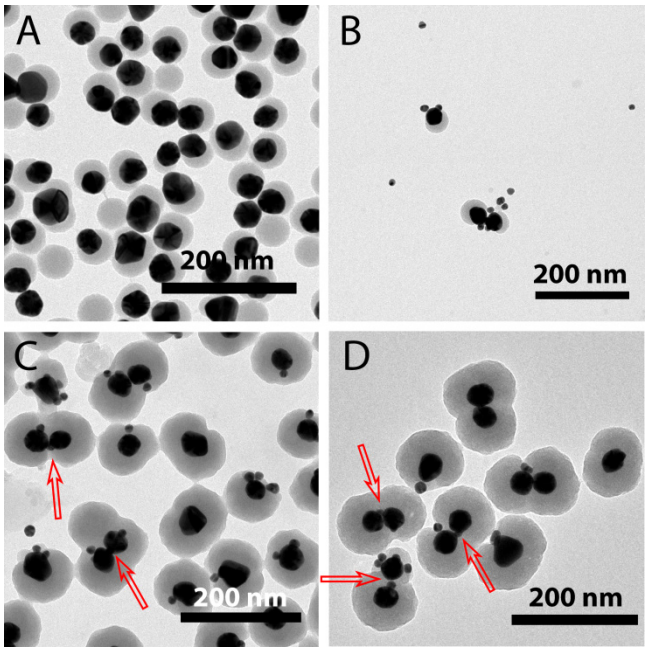

Figure 2. Representative TEM images of: A) Au_{40}(PAA-MBA@SiO_2) Janus particles; B) Intermediate structures formed after 5 min of assembly; C-D) Au-SiO_2 hybrid satellites. Red arrows indicate the position of Au_{15} acting as linkers for the Janus particles.

SERS measurements were carried out in water (upon transfer from ethanol) so as to minimize interference from the solvent and because it is a more suitable solvent toward experiments with cells. The concentrations of particles were estimated as $6.1{\cdot}10^{-11}$ M of Janus and $7.1{\cdot}10^{-9}$ M of Au_{15}, considering that no loses occurred during assembly, subsequent silica growth, and washing. In reality, non-adsorbed Au_{15} particles were removed during washing due to their smaller weight as compared to the hybrid satellites. 4-MBA was added during the synthesis of Au-SiO_2 Janus particles, at a concentration of $2.7{\cdot}10^{-5}$ M (35 molecules/nm^2), while RhB was incorporated during the assembly process, at a concentration of $9.6{\cdot}10^{-8}$ M (0.5 molecules/nm^2).

The SERS spectra of the hybrid satellites in water upon excitation with three different wavelengths (532, 633 and 785 nm) are shown in Figure 3. Upon 532 nm excitation (green spectrum), only scattered frequencies were detected that are related to the excitation of characteristic RhB vibrations (1620, 1580, 1560, 1340, 1280 and 1210 cm^{-1}). The peak positions are in good agreement with the modes reported for RhB adsorbed on micron sized Ag powder or on Ag nanoshells upon excitation with 514 and 633 nm.[56, 57] In contrast, totally different frequencies were scattered upon 785 nm excitation. The signals correspond to the excited vibrational states of the second Raman label, 4-MBA (1585, 1075, 1180 and 700 cm^{-1}, black curve), which do not overlap with the vibrations of RhB. Using the 633 nm excitation wavelength, a more complex spectrum was recorded in which the scattered 4-MBA frequencies dominate (black dots over the red curve in Figure 3) and less intense contributions from scattered RhB frequencies (marked by green dots). A control experiment using Janus particles and small Au_{15nm} spheres without aggregation was carried out to study the relation between the hybrid structure and the observed color-selective SERS behavior of the incorporated Raman tags. Strong SERS signals were recorded with 633 nm excitation whereas a much lower signal was detected in the 785 nm channel. As the signal originates from 4-MBA within the Janus building blocks, the intensities using the 785 nm channel are comparable in both systems (black spectrum in Figures 3 and S1). In the 532 nm channel only background fluorescence was detected, arising from unbound RhB molecules (see Figure S1). This clearly indicates that the assembly of satellites is required for RhB detection and that the SERS signal originates exclusively from molecules located within the hot spots between the central Janus particles and the small satellites. The strong SERS signal can be explained by the enhanced Raman cross section at 532 nm due to the RhB electronic resonance state around 550 nm.[56] These results demonstrate the ability of this system to act as a SERS switcher in water, allowing us to turn on or off the dye molecules at will by using different laser excitation colors. This offers the possibility for multiplex particle tracking via SERS using the excitation wavelength as an additional channel.

The experimental SERS enhancement factor (EF) of the hybrid satellite assemblies were calculated using the intensity ratio between SERS and Raman scattering (RS) signals, normalized by the number of contributing molecules (N), according to EF=$(I/N)_{SERS}$: $(I/N)_{RS}$.[58] Due to the low RS signals, the measurements were carried out from a solid powder and compared to a thin film assembly drop casted onto glass, leading to wavelength dependent EFs of $4.2x10^6$, $2.6x10^6$ and $4.9x10^6$ for 785, 633 and 532 nm respectively (more details in the SI).[59,60]

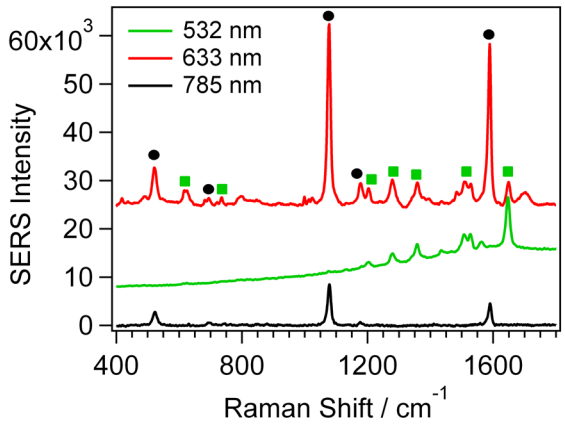

Figure 3. SERS spectra of hybrid satellites in water using 3 different laser wavelength lines: 532 nm (green line), 785 nm (black line) and 633 nm, (red line). The green dots indicate RhB vibrations and black dots the 4-MBA signature.

We next show that the molecular fingerprints of both RhB and 4-MBA can also be detected when the hybrid particles are internalized by cells in vitro. We selected the continuous macrophage cell line J774 because it is quickly adherent and actively phagocytoses (uptakes) particles. Both factors were important because of the small working volume of the sample and therefore long term incubation times of the cells with the particles were not possible, due to risk of complete evaporation of the media solution. Therefore, cells do not have an elongated form but are instead round (Figure 4A). Hybrid satellites were added to cells and SERS spectra at excitation

wavelengths of 532, 633 and 785 nm were collected after 1 h incubation from a single cell (Figure 4B-D). As the cell did not move noticeably over the measurement period, the same cell could be imaged with all excitation wavelengths. For each wavelength one individual SERS spectrum (green curve for 532 nm in B, black curve for 785 nm in C, and red curve for 633 nm in D) recorded at a single point within the cell was chosen and compared with the corresponding color-dependent reference from the hybrid satellites measured in solution without cells (grey lines in Figure 4B-D). The SERS spectra obtained in cells perfectly reflect the fingerprints of the RhB label at 532 nm, of the 4-MBA label at 785 nm and of both labels at 633 nm. No additional peaks were observed from the cell or the buffer solution under the present experimental conditions. As the reference spectra of hybrid satellites in solution were measured using 1800 or 1200 lines/mm gratings, whereas the cell maps were recorded with a 600 lines/mm grating (all wavelengths), a slight broadening of the SERS features in the cell compared to the reference sample was observed. The reference spectra were collected with long integration times of 10 s instead of 0.5 s, applied for the cell. Indeed, the signal-to-noise ratio of hybrid satellites in the cell strongly decreases but is still high enough to record the less intense vibrations.

The intensity distribution of the characteristic vibrations at 1620 cm^{-1} (RhB) and 1080 cm^{-1} (4-MBA) in the SERS maps appear to show that the hybrid satellites filled the interior of the macrophage (Figure 4B-D). By conducting SERS mapping in either the streamline mode (line focus) or the mapping mode using short step sizes (≤1 µm), a higher level of lateral resolution for the hybrid satellites could be obtained (Figure S2). Importantly, although the cells were not fully adhered and the incubation times between cells and particles were short (1 h), endocytosis of particles was noted at high levels and was not affected by washing. It is possible that part of the SERS signal came from particles associated to the cell membrane, however bearing in mind the phagocytic nature of J774's, such levels should be negligible.

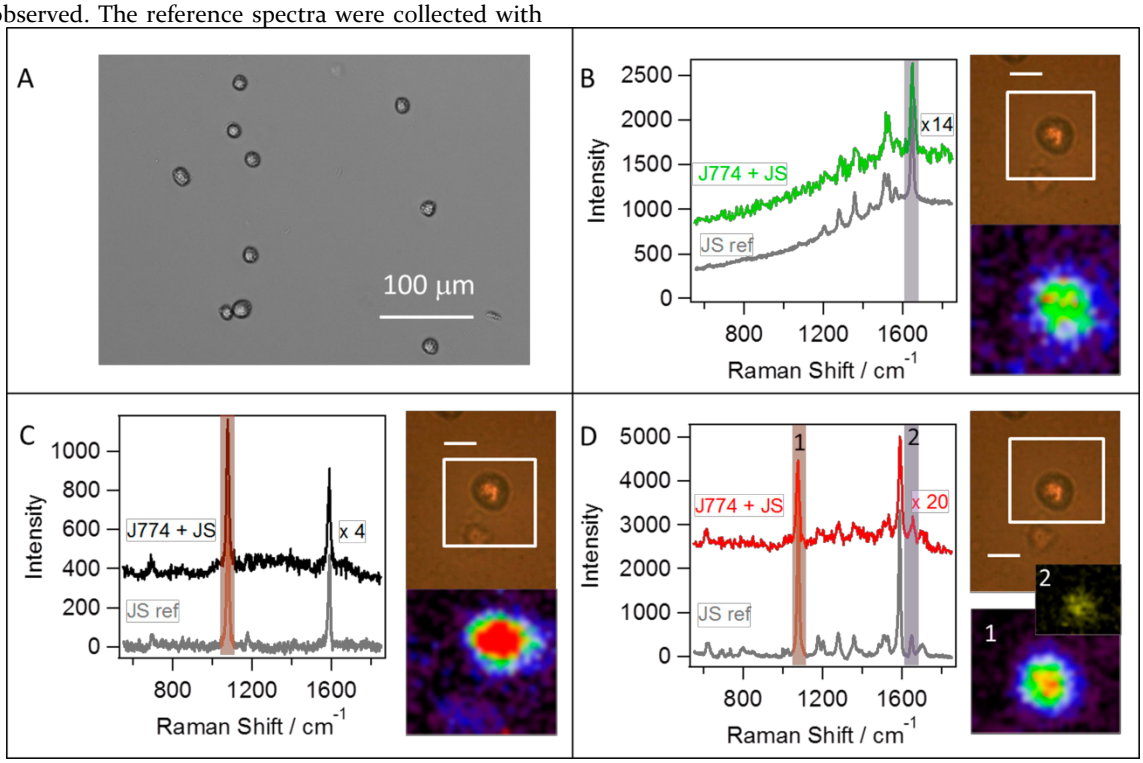

Figure 4. A: Representative transmitted light image of the macrophage cell line J744 before incubation with hybrid satellites; B-D: color-dependent SERS spectra of J744 (left), white-light image and SERS maps (right) recorded 1 h after incubation with hybrid satellites from the same single cell, at 532 nm (B), 785 nm (C) and 633 nm (D). To facilitate comparison of the cell spectra (J774+JS, green, black and red curves) with the corresponding reference spectra from hybrid satellites in water at the same wavelengths (JS ref, grey curves), the SERS intensities were multiplied by: 14 (B), 4 (C) and 20 (D). SERS maps for each excitation color were created by plotting the intensity of the selected mode (marked in the SERS spectrum with an orange bar for 4-MBA at 1078 cm^{-1} and a purple bar for RhB at 1617 cm^{-1}) within the selected area (marked by the white frame in the white-light image) using a color code from black (low intensity) to red (highest intensity); the color code in the SERS map 2 (RhB/1617 cm^{-1}) in D ranged from black (low) to bright yellow (high intensity). The white scale bar corresponds to 20 µm.

CONCLUSIONS

We have shown that hybrid satellites composed of silica and gold nanoparticles can be encoded with two different dyes and applied for multiplex labeling applications, both in aqueous solutions and in color-sensitive SERS bioimaging. This concept should be interesting for applications where the independent detection of two different components using the same analytical technique is of advantage. Such a scenario is potentially interesting, e.g. in drug delivery schemes. Through replacement of RhB by a drug molecule and intro-

duction of a disassembly step of the hybrid satellites, drug tracking and release could be directly controlled via SERS signal intensity using the green laser excitation. Additionally, tracking and fate of the delivery medium, i.e. the Au nanoparticles, can be independently monitored by the SERS fingerprint of the fixed residue molecule just by switching to another excitation line. These assemblies are thus a proof of concept showing the capabilities of these structures, but the design can be varied to extend their possible applications. For example, the outer silica layer could be modified to make these structures specifically bind to cancer cells.

ASSOCIATED CONTENT

SERS control experiment and SERS mapping of cells. This material is available free of charge via the Internet at http://pubs.acs.org.

AUTHOR INFORMATION

Corresponding Author

* Email: *llizmarzan@cicbiomagune.es*

ACKNOWLEDGMENT

Funding from the European Research Council (ERC Advanced Grant #267867 Plasmaquo) and the Spanish MINECO (Grant MAT2013-46101-R) is gratefully acknowledged. D.R.-F. acknowledges receipt of an F.P.U. scholarship from the Spanish Ministry of Education and Culture. Authors thank A. Ruiz de Angulo Dorronsoro for guidance on cell experiments preparation.

REFERENCES

1. Fleischmann, M.; Hendra, P. J.; McQuillan, A. J. *Chem. Phys. Lett.* **1974**, *26*, 163.
2. Albrecht, M. G.; Creighton, J. A. *J. Am. Chem. Soc.* **1977**, 99, 5215.
3. Jeanmaire, D. L.; van Duyne, R. P. *J. Electroanal. Chem.* **1977**, *84*, 1.
4. Pettinger, B.; Wenning, U. *Chem. Phys. Lett.* **1978**, *56*, 253.
5. Creighton, J. A.; Blatchford, C. G.; Albrecht, M. G. *J. Chem. Soc. Faraday Trans. II* **1979**, *75*, 806.
6. Arvind, P. K.; Nitzan, A.; Metiu, H. *Surf. Sci.* **1981**, *110*, 189.
7. Xu, H.; Aizupurua, J.; Käll, M.; Apell, P. *Phys. Rev. E* **2000**, *62*, 4318.
8. Sonntag, M. D.; Klingsporn, J. M.; Zrimsek, A. B.; Sharma, B.; Ruvuna, L. K.; Van Duyne, R. P. *Chem. Soc. Rev.* **2014**, *43*, 1230.
9. Jiang, J.; Bosnick, K.; Maillard, M.; Brus, L. *J. Phys. Chem. B* **2003**, *107*, 9964.
10. Le Ru, E. C.; Etchegoin, P. G.; Meyer, M. *J. Chem. Phys.* **2006**, *125*, 204701.
11. Futamata, M.; Maruyama, Y.; Ishikawa, M. *J. Mol. Struct.* **2005**, *735*, 75.
12. Futamata, M. *Faraday Discuss.* **2006**, *132*, 45.
13. Sasic, S.; Itoh, T.; Ozaki, Y. *J. Raman Spectrosc.* **2005**, *36*, 593.
14. Fang, Y.; Seong, N.H.; Dlott, D.D. *Science* **2008**, *321*, 388.
15. Stranahan, S. M.; Willets, K. A. *Nano Lett.* **2010**, *10*, 3777.
16. Isola, N. R.; Stokes, D. L.; Vo-Dinh, T. *Anal. Chem.* **1998**, *70*, 1352.
17. Graham, D.; Mallinder, B. J.; Whitcombe, D.; Watson, N. D.; Smith, W. E. *Anal. Chem.* **2002**, *74*, 1069.
18. Cao, Y.-W. C.; Jin, R. C.; Mirkin, C. A. *Science* **2002**, *297*, 1536.
19. Ni, J.; Lipert, R. J.; Dawson, G. B.; Porter, M. D. *Anal. Chem.* **1999**, *71*, 4903.
20. Cao, Y.-W. C.; Jin, R. C.; Mirkin, C. A. *J. Am. Chem. Soc.* **2003**, *125*, 14676.
21. Grubisha, D. S.; Lipert, R. J.; Park, H. Y.; Driskell, J.; Porter, M. D. *Anal. Chem.* **2003**, *75*, 5936.
22. Kneipp, J.; Kneipp, H.; Rajadurai, A.; Redmond, R. W.; Kneipp, K. *J. Raman Spectrosc.* **2009**, *40*, 1.
23. Kennedy, D. C.; Hoop, K. A.; Tay, L.-L.; Pezacki, J. P. *Nanoscale* **2010**, *2*, 1413.
24. Pallaoro, A.; Braun, G. B.; Reich, N. O.; Moskovits, M. *Small* **2010**, *6*, 618.
25. Wang, Y.; Seebald, J. L.; Szeto, D. P.; Irudayaraj, J. *ACS Nano* **2010**, *4*, 4039.
26. Mulvaney, S. P.; Musick, M. D.; Keating, C. D.; Natan, M. J. *Langmuir* **2003**, *19*, 4784.
27. Doering, W. E.; Nie, S. *Anal. Chem.* **2003**, *75*, 6171.
28. McCabe, A. F.; Eliasson, C.; Prasath, R. A.; Hernandez-Santana, A.; Stevenson, L.; Apple, I.; Cormack, P. A. G.; Graham, D.; Smith, W. E.; Corish, P.; Lipscomb, S. J.; Holland, E. R.; Prince, P. D. *Faraday Discuss.* **2006**, *132*, 303.
29. Faulds, K.; McKenzie, F.; Smith, W. E.; Graham, D. *Angew. Chem. Int. Ed.* **2007**, *46*, 1829.
30. Su, X.; Zhang, J.; Sun, L.; Koo, T.-W.; Chan, S.; Sundararajan, N.; Yamakawa, M.; Berlin, A. A. *Nano Lett.* **2005**, *5*, 49.
31. Brown, L.; Doorn, S. K. *Langmuir* **2008**, *24*, 2277.
32. Braun, G. B.; Pavel, I.; Morill, A. R.; Seferos, D. S.; Bazan, G. C.; Reich, N. O.; Moskovits, M. *J. Am. Chem. Soc.* **2007**, *129*, 7760.
33. Fabris, L.; Dante, M.; Nguyen, T.-Q.; Tok, J. B.-H.; Bazan, G. C. *Adv. Funct. Mater.* **2008**, *18*, 18.
34. Braun, G. B.; Lee, S.J.; Laurence, T.; Fera, N.; Fabris, L.; Bazan, G. C.; Moskovits, M.; Reich, N. O. *J. Phys. Chem. C* **2009**, *113*, 13622.
35. Xia, X.; Li, W.; Zhang, Y.; Xia, Y. *Interface Focus* **2013**, 3, 20120092.
36. Qian, X.; Peng, X.-H.; Ansari, D. O.; Yin-Goen, Q.; Chen, G. Z.; Shin, D. M.; Yang, L.; Young, A. N.; Wang, M. D.; Nie, S. *Nature Biotechnology* **2008**, *26*, 83.
37. Zavaleta, C. L.; Smith, B. R.; Walton, I.; Doering, W.; Davis, G.; Shojaei, B.; Natan, M. J.; Gambhir, S. S. *Procs. Nat. Acad. Sci.* **2009**, *106*, 13511.
38. Gellner, M.; Kömpe, K.; Schlücker, S. *Anal. Bioanal. Chem.* **2009**, *394*, 1839.
39. Maiti, K. K.; Dinish, U. S.; Samanta, A.; Vendrell, M.; Soh, K.-S.; Park, S.-J.; Olivo, M.; Chang, Y.-T. *Nano Today* **2012**, *7*, 85.
40. von Maltzahn, G.; Centrone, A.; Park, J.-H.; Ramanathan, R.; Sailor, M. J.; Hatton, T. A.; Bhatia, S. N. *Adv. Mater.* **2009**, *21*, 3175.
41. Xiao, M.; Nyagilo, J.; Arora, V.; Kulkarni, P.; Xu, D.; Sun, X.; Dave, D. P. *Nanotechnology* **2010**, *21*, 035101.
42. Kircher, M. F.; de la Zerda, A.; Jokerst, J. V.; Zavaleta, C. L.; Kempen, P. J.; Mittra, E.; Pitter, K.; Huang, R.; Campos, C.; Habte, F.; Sinclair, R.; Brennan, C. W.; Mellinghoff, I. K.; Holland, E. C.; Gambhir, S. S. *Nature Med.* **2013**, *18*, 829.
43. Nima, Z. A.; Mahmood, M.; Xu, Y.; Mustafa, T.; Watanabe, F.; Nedosekin, D. A.; Juratli, M. A.; Fahmi, T.; Galanzha, E. I.; Nolan, J. P.; Basnakian, G.; Zharov, V. P.; Biris, A. S. *Sci. Rep.* **2014**, *4*, 4752.
44. Wustholz, K. L.; Henry, A.-I.; McMahon, J. M.; Freeman, R. G.; Valley, N.; Piotti, M. E.; Natan, M. J.; Schatz, G. C.; Van Duyne, R. P. *J. Am. Chem. Soc* **2010**, *132*, 10903.
45. Kleinman, S. L.; Sharma, B.; Blaber, M. G.; Henry, A.-I.; Valley, N.; Freeman, R. G.; Natan, M. J.; Schatz, G. C.; Van Duyne, R. P. *J. Am. Chem. Soc.* **2013**, *135*, 301.

46. Cha, H.; Yoon, J. H.; Yoon, S. *ACS Nano* **2014**, *8*, 8554.
47. Rodríguez-Fernández, D.; Liz-Marzán, L. M. *Part. Part. Syst. Charact.* **2013**, *30*, 46.
48. Turkevich, J.; Stevenson, P. C.; Hillier, J. *Discuss. Faraday Soc.* **1951**, *11*, 55.
49. Graf, C.; Vossen, D. L. J.; Imhof, A.; van Blaaderen, A. *Langmuir* **2003,** *19,* 6693.
50. Rodríguez-Fernández, D.; Altantzis, T.; Heidari, H.; Bals, S.; Liz-Marzán, L. M. *Chem. Commun.* **2014**, *50*, 79.
51. Chen, T.; Chen, G.; Xing, S.; Wu, T.; Chen, H. *Chem. Mater.* **2010**, *22*, 3826.
52. Qian, X.; Emory, S. R.; Nie, S. *J. Am. Chem. Soc.* **2012**, *134*, 2000.
53. Michaels, A. S.; Morelos, O. *Ind. Eng. Chem.* **1955**, *47*, 1801
54. Liz-Marzán, L. M. *Langmuir* **2006**, *22*, 32.
55. Stöber, W.; Fink, A.; Bohn, E. *J. Colloid Interface Sci.* **1968**, *26*, 62.
56. Kim, K.; Lee, Y. M.; Lee, J. W.; Shin, K. S. *Langmuir* **2009**, *25*, 2641.
57. Kim, K.; Lee, H. B.; Lee, Y. M.; Shin, K. S. *Biosens. Bioelectr.* **2009**, *24*, 1864.
58. Cai, W. B.; Ren, B.; Li, X. Q.; She, C. X.; Liu, F. M.; Cai, X. W.; Tian, Z. Q. *Surf. Sci.* **1998**, 406, 9.
59. Khan, M. A.; Hogan, T. P.; Shanker, B. *J. Raman Spectros.* **2008**, 39, 893.
60. Jiang, X.; Zhang, L.; Wang, T.; Wan, Q. *J. Appl. Phys.* **2009**, 106, 104316.

Table of Contents Graphics